

MS3D: Leveraging Multiple Detectors for Unsupervised Domain Adaptation in 3D Object Detection

Darren Tsai, Julie Stephany Berrio, Mao Shan, Eduardo Nebot and Stewart Worrall

Abstract—We introduce Multi-Source 3D (MS3D), a new self-training pipeline for unsupervised domain adaptation in 3D object detection. Despite the remarkable accuracy of 3D detectors, they often overfit to specific domain biases, leading to suboptimal performance in various sensor setups and environments. Existing methods typically focus on adapting a single detector to the target domain, overlooking the fact that different detectors possess distinct expertise on different unseen domains. MS3D leverages this by combining different pre-trained detectors from multiple source domains and incorporating temporal information to produce high-quality pseudo-labels for fine-tuning. Our proposed Kernel-Density Estimation (KDE) Box Fusion method fuses box proposals from multiple domains to obtain pseudo-labels that surpass the performance of the best source domain detectors. MS3D exhibits greater robustness to domain shifts and produces accurate pseudo-labels over greater distances, making it well-suited for high-to-low beam domain adaptation and vice versa. Our method achieved state-of-the-art performance on all evaluated datasets, and we demonstrate that the choice of pre-trained source detectors has minimal impact on the self-training result, making MS3D suitable for real-world applications. Our code is available at <https://github.com/darrenjkt/MS3D>.

I. INTRODUCTION

3D object detection is a vital component of AVs, serving as a fundamental building block for critical downstream tasks such as path prediction. The field has benefited greatly from the availability of large-scale AV datasets [1]–[4], which have fueled research in the development of 3D detectors. Unfortunately, directly applying these 3D detectors to new datasets results in suboptimal performance due to domain shift. Factors such as variations in lidars, geographic regions, scenarios, and sensor setups pose significant challenges for the effective testing and deployment of 3D object detectors. Traditionally, the approach to improving detectors for new datasets is to manually annotate the data for fine-tuning the existing detector. However, this approach is both costly and labour-intensive, therefore highlighting the need for effective approaches to adapt 3D detectors trained on labelled source domains to new, unlabelled target domains. This task is called unsupervised domain adaptation (UDA).

In this paper, we introduce Multi-Source 3D (MS3D), a novel pipeline for generating high-quality pseudo-labels on an unlabelled dataset for self-training in the context of UDA for 3D Object Detection. Unlike existing methods, MS3D takes advantage of the collective knowledge of multiple

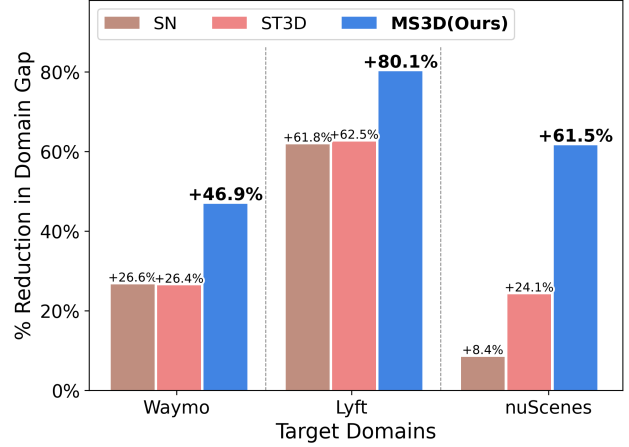


Fig. 1: Performance of MS3D compared to SN [5] and ST3D [6] for Lyft \rightarrow Waymo, Waymo \rightarrow Lyft and Waymo \rightarrow nuScenes (from left to right). Graph shows how much these methods have reduced the domain gap (in AP_{3D} at $IoU=0.7$) between source-only (no UDA, i.e., 0%), and fine-tuned with target domain labels (i.e., 100%).

detectors to generate pseudo-labels on a single novel dataset. Moreover, by accumulating frames, MS3D improves the robustness of detection boxes on static objects.

One of the key benefits of MS3D is its ability to adapt robustly to a wide range of domain shifts by leveraging the expertise of multiple detectors. When using self-training in the standard single source-target domain adaptation setting, the choice of source dataset and detector can significantly impact fine-tuning performance. In practice, it is challenging to evaluate and identify the optimal source dataset and detector due to lack of labelled data on new target datasets. However, with MS3D, the choice of source dataset and detector has minimal impact on the final performance. We demonstrate that the combined pseudo-labels produced are of higher quality than those of the optimal individual source-trained detector and as a result, our fine-tuned performance outperforms state-of-the-art single-source UDA methods as shown in Fig. 1.

Our proposed approach is built upon two fundamental observations. Firstly, we recognize that different detectors trained on various datasets possess distinct expertise. For instance, a detector trained on the Waymo dataset may be better suited for a specific novel dataset compared to a detector trained on nuScenes, and vice versa. Secondly, we observe that by utilizing temporal point clouds (i.e., multi-frame accumulation), we can aggregate various perspectives to gain a more comprehensive understanding of static objects' complete geometry, leading to more accurate bounding

This work has been supported by the Australian Centre for Field Robotics (ACFR) and ARC LIEF grant LE200100049 Whopping Volta GPU Cluster - Transforming Artificial Intelligence Research. (Corresponding author: Darren Tsai.)

The authors are with the Australian Centre for Field Robotics (ACFR) at the University of Sydney (NSW, Australia). E-mails: {d.tsai, j.berrio, m.shan, e.nebot, s.worrall}@acfr.usyd.edu.au

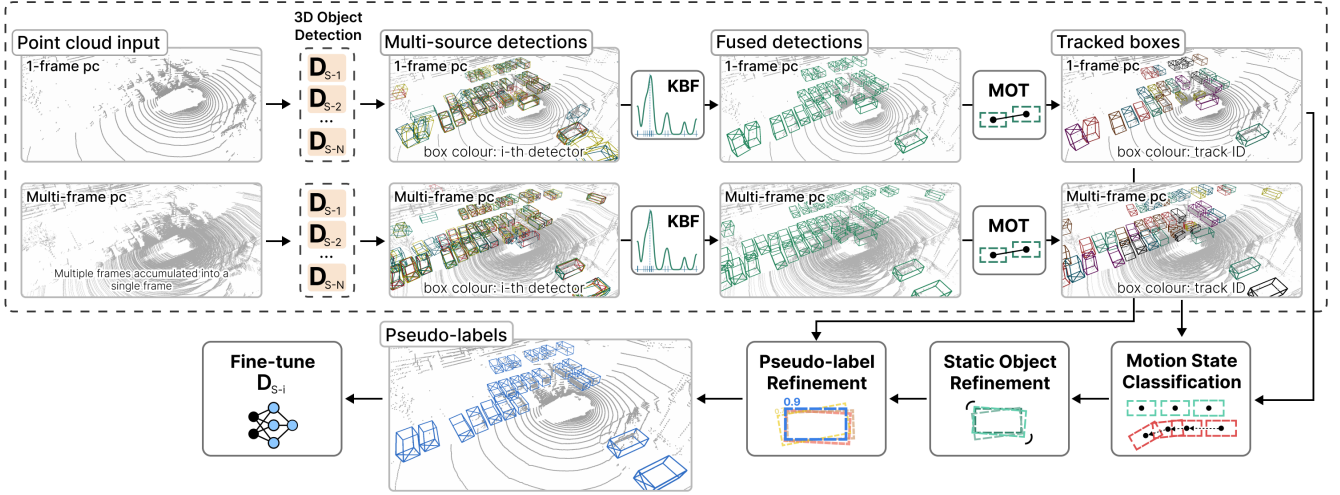


Fig. 2: **The MS3D self-training pipeline.** Given a set of N pre-trained 3D detectors from multiple source domains D_{S-i} where $i = 1, 2, \dots, N$, we generate detections for both 1-frame and multi-frame accumulated point clouds, and combine them with our KBF. Thereafter, we feed the sequence frames into a 3D tracker for generating trajectories of both 1-frame and multi-frame boxes. Finally, we refine static object boxes to get our final pseudo-labels for fine-tuning any pre-trained detector D_{S-i} . Visualized in this figure is our MS3D pipeline for Waymo/Lyft \rightarrow nuScenes.

boxes [3], [7]–[9].

In real-world scenarios, Multi-Source Domain Adaptation (MSDA) is a practical and effective approach for adaptation to a target domain. The availability of multiple source domains enables us to harness diverse knowledge and improve the overall performance of 3D object detectors on unlabelled datasets. Fortunately, there are many large-scale datasets that can be leveraged for MSDA in 3D object detection, including nuScenes, Waymo, and Lyft, among others. By incorporating the rich information from these sources, we can significantly reduce the domain shift and improve the generalization ability of 3D detectors.

A naive approach to combining multiple source-trained detectors on a new domain is to select the detection box produced by the most confident detector. However, this method neglects potentially valuable information provided by the other detectors, and it is possible that the most confident detector is not necessarily the most accurate. Instead, we propose KDE Box Fusion (KBF), a more robust box-fusion strategy that utilizes KDE to consider each detector’s proposal and enhance pseudo-label quality. We note that KBF can also be applied for detector ensembling in a supervised setting.

Point cloud accumulation has gained popularity as a promising direction for improving single-frame detection through densification. Yang et al. [7] demonstrated that concatenating 4 point cloud frames had the optimal performance boost before it started to deteriorate with more frames for the Waymo dataset. However, they observe that for static and slow objects, accumulating more than 4 frames continued to improve detection performance. Qi et al. [8] showed that accumulating 100+ frames of a sequence can be effectively utilized by separating static and dynamic vehicle box refinement. To capitalize on these findings, we explore the use of multi-frame detection in the context of UDA to refine the box localization of static objects. Furthermore,

by extending the static boxes of parked vehicles in both directions temporally, we obtain precise pseudo-labels for objects located beyond 50m from the ego-vehicle.

Contributions. Our main contribution is MS3D, a multi-source domain adaptation approach for 3D object detection that leverages multiple source domain experts and temporal information to generate high quality pseudo-labels for self-training. The benefits of our approach are:

- **Robust:** By combining the expertise of different detectors trained on various source domains, MS3D is more robust against domain shifts.
- **Versatile and Scalable:** MS3D is easily combined with multiple and various types of pre-trained 3D detectors to further boost pseudo-label quality.
- **Improved Pseudo-labels:** MS3D self-trained models can obtain state-of-the-art performance regardless of the source pre-trained model chosen for self-training. This is because our fused pseudo-labels consistently outperform the best individual source domain detector.
- **Speed:** MS3D does not add any processing latency during inference, ensuring it can be used in real-time applications.
- **Detection Performance:** MS3D achieves state-of-the-art on all UDA settings presented.

II. RELATED WORK

3D object detection. A significant portion of the current research in 3D detection is concentrated on single-frame detection. Within this, many works propose to enhance the feature representation of point clouds, by proposing feature representations that can be classified as voxel-based [10], [11], point-based [12], [13], or a combination of both [14]. Recent works have delved into the use of temporal information, where some works have shown that a simple multi-frame concatenation can already outperform single-frame detection [3], [7], [15]. However, this improvement is limited and the performance deteriorates for longer sequences. To

address this challenge, a few studies have focused on developing spatio-temporal feature encoding strategies that fully leverage information from longer sequences [7], [9]. Another strategy is to separately encode sequences of dynamic and static object [8] for box refining.

Unsupervised Domain Adaptation. Research in UDA for 3D object detection has been predominantly focused on adapting a single detector, trained on a labelled domain (source dataset), to a new domain (target dataset). UDA approaches can be categorised into adversarial methods [16], [17], domain-invariant feature representation [18], self-training [19], mean teacher [20], amongst others. More specifically in 3D object detection, prior research showcased successful adaptation of detectors from larger-car datasets like Waymo and nuScenes, to smaller-car datasets like KITTI [5], [6], [21]–[23]. A popular direction for this topic is to use self-training, where the focus is on generating high quality pseudo-labels for fine-tuning the source-trained detector [6], [24], [25]. ST3D [6] employed random object scaling augmentation within a self-training framework for more precise pseudo-labels for adaptation to the KITTI dataset. [26] improved ST3D for adapting from a 64 to 32-beam dataset via their generative method of emulating a pseudo 32-beam lidar.

Multi-Source Domain Adaptation. MSDA is an emerging variant of UDA that builds on UDA techniques while incorporating new techniques that leverage multiple source domains [27], [28]. For example, [29] uses style transfer to reduce the discrepancy of multiple source image styles in a collaborative learning framework. [30] proposes to align the feature space of multiple sources through an exponential moving average parameter combination for object detection. Recently, [31] extended this to 3D object detection with a focus on learning domain-agnostic features from multiple source datasets to improve detector generalization. To the best of our knowledge, [31] is the only attempt at MSDA for 3D object detection. Our approach differs from theirs in that we focus on combining detectors rather than combining datasets, and we accomplish this without modifying detector architecture or using source domain data (i.e., source-free). We focus on an early-stage fusion of multiple sources within a self-training framework. Our box-fusion strategy shares similarities with popular ensembling box filtering strategies such as NMS [32], Soft-NMS [33] and Weighted Box Fusion (WBF) [34]. In particular, WBF uses confidence scores as weights to determine new box corners in image detection. However, we find that applying WBF to the 3D space is suboptimal compared to our proposed KBF.

III. MULTI-SOURCE 3D

A. Problem Statement

In unsupervised MSDA, we have multiple M labelled source domains S_1, S_2, \dots, S_M and a single unlabelled target domain T . In our context, each i -th source $S_i = \{(p_{S,i}, L_{S,i})\}_i^N$ is a detector that has been trained on a point cloud dataset $p_{S,i}$ with annotations $L_{S,i}$. This source-trained detector's box predictions on the k -th frame of the unlabelled target dataset is denoted as $\{B_{T,i}^k\}_i^N$. Our goal is combine box predictions from each source-trained detector and utilize temporal information to robustly localize and classify objects

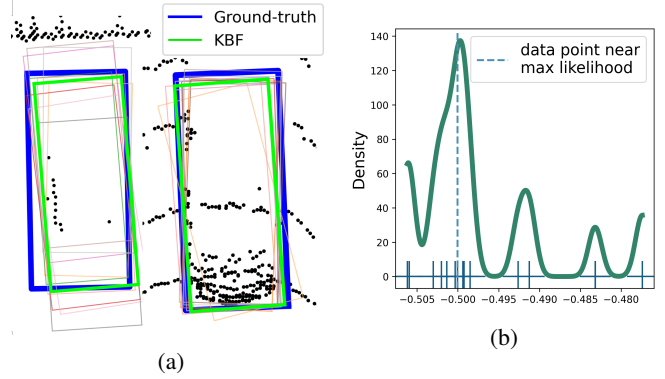


Fig. 3: (a) Fused TTA predictions of 4 source detectors (multi-coloured boxes) with KDE Box Fusion (KBF); (b) Example of how we select the best rotation of multiple boxes with KDE.

in 3D for each frame. We assume that the vehicle ego-pose is known in world coordinates for ego-motion compensation. Fig. 2 illustrates our proposed pipeline, which we will introduce in the following sections.

B. Fusing multiple sources

Initial Pseudo-labels. In order to enhance the resilience of our model against domain shifts in the unlabelled target domain, we use different types of detectors and source datasets for a greater range of knowledge. For example, with Waymo as our target domain, we employ both nuScenes and Lyft source domains, with two types of detectors, namely SECOND [10] and CenterPoint [35]. We notice that Lyft's lidar scan pattern is similar to that of Waymo, which could give Lyft-trained detectors an edge over nuScenes-trained detectors in certain scenarios. Additionally, different detectors possess varying areas of expertise. For instance, SECOND is adept at estimating object dimensions for axis-aligned objects due to its anchor boxes, whereas CenterPoint performs better with objects that are not axis-aligned [35].

We take advantage of a detector's full expertise by using two augmentations for Test Time Augmentation (TTA) - random world flip (RWF) across x and y axes, and random world rotation (RWR) in the range $[-\pi, \pi]$. For each source detector we run four permutations: no TTA, RWF, RWR, RWF+RWR, which gives $\{B_{T,i}^k\}_i^4$ for the i -th source detector on the k -th frame which we then fuse with KBF as follows.

KDE Box Fusion. The backbone of our KBF method, $\kappa(\cdot)$, is KDE [36], which is capable of estimating a probability density function (PDF) using a kernel function shown in Eq. (1). KDE places a kernel K at each data point x_i which sums to give the final PDF estimate $\hat{f}(x)$ as shown in Fig. 3b. A weight w_i for each data point and a kernel bandwidth h can be adjusted for fine-tuning the PDF estimate.

$$\hat{f}(x) = \frac{1}{h} \sum_{i=1}^N w_i K\left(\frac{x - x_i}{h}\right) \quad (1)$$

In 3D object detection, a predicted box is parameterised by its centre (c_x, c_y, c_z) , dimensions (l, w, h) , heading θ_y and a confidence score s . Regardless of the localization accuracy, each box carries potentially valuable information. For example, we observe that a box with poor heading

estimation may have accurate object dimensions. Therefore to combine the information of every box proposal, we opt to fuse the centre, length, width, height and heading separately.

To merge boxes, we first create a KD-Tree with the box centroids. We identify matching boxes by querying for sets of boxes that are within a certain radius of each other. We compute KDE separately for the centroid, dimensions and score, then select the peak value of each of their PDF. We take the sine of the heading, $\sin(\theta_y)$, to ensure rotational continuity before applying KDE. We found empirically that selecting rather than combining box headings produces the best result. Therefore, we choose the box heading with the highest likelihood based on the output PDF. For each box parameter we use a Gaussian kernel and use the predicted box confidence score as weights. Given the set of 1-frame detections from i source detectors, we fuse them with KBF to obtain boxes $B_{1f} = \kappa(\{B_{i,1f}\})$ for each frame k .

C. Utilizing Temporal Information for Static Vehicles

In urban city environments, parked vehicles are common and often are completely static for long periods. Car parks in particular are often present in datasets and provides an abundance of viewpoints for various types of vehicles. With this in mind, we use multi-frame detection to leverage the additional viewpoints provided by accumulated point clouds to better localize static vehicles. For multi-frame detection, the input point cloud p_t^k for frame k is the stacking of N historical point clouds with the point cloud at time t where each historical point cloud has been transformed to the ego-frame at time t . With a 10Hz lidar, each point cloud is 0.1s apart, and the accumulated point cloud can be represented as $p_t^k = \{p_t, p_{t-0.1}, p_{t-0.2}, \dots, p_{t-N(0.1)}\}$. By feeding the source detector with p_t^k , it can utilize the increased point density to improve the accuracy of box localization, particularly for static objects that may be occluded or located at a distance as shown in Fig. 4. In particular, we follow [9] to use $N = 16$ frames for detection for a trade-off between TTA inference time and point cloud density. We use the same TTA permutations and combine box predictions with KBF, $B_{16f} = \kappa(\{B_{i,16f}\})$, as in Section III-B.

D. Motion State Classification

To assign temporally consistent boxes for static vehicles, we associate detection boxes across frames to classify the motion state of the object. To accomplish this, we transform all boxes to world coordinates with known sensor poses. Thereafter, we utilize a tracking-by-detection, Kalman Filter-based tracker [37] which is an implementation variant of [38] to generate box trajectories for both 1-frame, T_{1f} , and 16-frame, T_{16f} , predictions. Following [8], we classify the tracklets as either static or dynamic based on pre-defined thresholds of begin-to-end distance and box centre variance.

Nonetheless, this is not sufficient in classifying T_{16f} due to predictions on the motion trails of dynamic objects in 16-frame detection. We observe that when two dynamic vehicles are driving in the same lane at a similar speed, their motion tails often overlap, leading to a false 'static' classification. A simple approach to replacing static boxes would be to rely solely on the motion classification of T_{1f} and replace static objects with their corresponding T_{16f} boxes. However, this

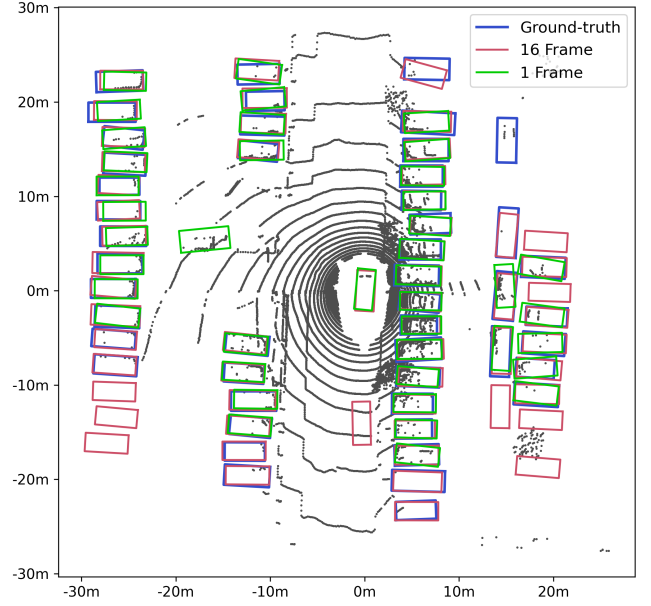


Fig. 4: 1-frame KBF boxes compared to 16-frame KBF boxes on the nuScenes dataset with detectors trained on Waymo/Lyft as the source domain. Visualized is a 1-frame point cloud.

approach is suboptimal since 1-frame detection often detects less static objects at a distance than 16-frame detection for certain target datasets as shown in Fig. 4, causing us to overlook valuable 16-frame boxes as a result.

To improve the accuracy of T_{16f} motion classification, we make a key observation: in 3D space, dynamic objects cannot occupy the same space as an object that is static throughout the sequence. This means that the trajectory of a dynamic object will never overlap with that of a parked vehicle. To take advantage of this, we use T_{1f} to identify all dynamic objects in frame k , and project their entire trajectory T_{1f} into frame k . This effectively identifies drivable areas and enables us to filter out wrongly classified static boxes through comparing IOU-matched T_{1f} and T_{16f}^k boxes. If either T_{1f} or T_{16f}^k is labeled as dynamic, we classify the object as dynamic. While this might lead to more objects falsely classified as dynamic, it prevents harmful extrapolation of vehicles that are only temporarily stationary.

E. Multi-frame Static Object Refinement

In theory, a static vehicle's position in world coordinates should remain constant throughout an entire sequence, allowing us to assign the vehicle a single bounding box for the sequence. However, we observed that selecting a single static box and projecting it across all frames in the sequence showed perfect localization in some frames but poor localization in others. To investigate this, we projected all ground-truth boxes of a sequence into a single frame in world coordinates, shown in Fig. 5, and noticed that many parked vehicles did not have a single consistent box across all frames. For example, when we took the 0-th frame's box, $B_{GT,0}$, of a static vehicle and projected it into the 100-th frame where the static vehicle was still visible, we noticed that $B_{GT,0}$ excluded many, and sometimes all of the

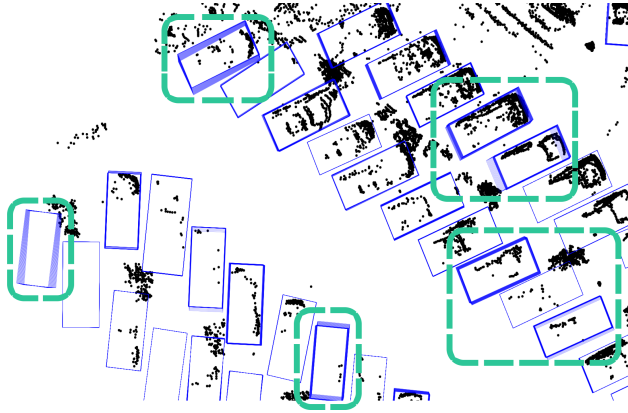


Fig. 5: All boxes of a Waymo sequence projected into a single frame in world coordinates. In the dotted teal boxes we show that some static vehicles do not have a single consistent box for the whole sequence due to ego-pose drift.

vehicle’s points. This highlighted the fact that in practice, the position of static objects drift due to ego-pose error and therefore using a single bounding box for the whole sequence is insufficient for static vehicle labelling.

This ego-pose drift was observed in multiple datasets such as nuScenes, Waymo, Lyft and KITTI with some datasets worse than others. To address this, we propose to use KBF on H historical observation frames, $\kappa(\{T_{16f}\}_{k-H}^k)$, to obtain a static box for the k -th frame instead of using all frames. This gives us a static box $\{B_{static}^k\}_k^N$ for each k -th frame with a score determined by $\max(\alpha, s_{static}^k)$ where α is a minimum score threshold and s_{static}^k is the fused score of $\{B_{static}^k\}_k^N$.

To extend the range of pseudo-labels, we assume that static vehicles with sufficiently long tracks will remain static throughout the sequence. Many source-trained detectors can only reliably identify vehicles within a closer range for a new target domain. Therefore, we propagate the first and last KBF boxes of static vehicles through historical and future frames, respectively, under the assumption that they remain static. To reduce the increase in false positives resulting from this propagation, we decay the confidence score of the propagated boxes by β for each frame that it is propagated. For certain datasets, we found that updating the pseudo-labels in the self-training process to refine these propagated boxes can give a bump in performance.

F. Pseudo-Label Refinement

In the UDA setting, higher point density with 16-frame accumulation does not necessarily lead to improved detection at close ranges compared to 1-frame detections. This is partly because densified point clouds may accentuate differences in scan patterns, and also because static boxes can be susceptible to ego-pose drift, which negatively affects localization accuracy. To address this issue and combine all box proposals, we employ Non-Maximum Suppression (NMS) to allow confident single frame detections to replace 16-frame static boxes. We project the following into the scene and apply NMS for filtering: (1) 1-Frame KBF boxes; (2) T_{1f} tracked boxes; and (3) Static object boxes, $\{B_{static}^k\}_k^N$. Finally, we remove any pseudo-labels with less than 1 point inside their box. By including T_{1f} tracked boxes, we can

Dataset	Lidar Beams	Size	Rain	Night	Country
nuScenes	1×32	34,149	Yes	Yes	USA, Singapore
Waymo	1×64 + 4×200	192,484	Yes	Yes	USA
Lyft	1×40 or 64 + 2×40	18,634	No	No	USA

TABLE I: Overview of each dataset. Country refers to the country in which the dataset was collected.

interpolate missing detections and extrapolate for farther ranges in a similar manner to [24].

IV. EXPERIMENTS

A. Setup

Datasets. Many works have addressed the object size domain gap and improved adaptation to the KITTI dataset [5], [6], [21], [23], [24]. However, other factors such as scan pattern, weather and geographical differences have a significant impact on the domain gap. To focus on this, we select datasets with similar object sizes: Waymo [2], Lyft [4] and nuScenes [3], summarised in Table I, for our experiments.

Methods. We compare MS3D with the following methods: (1) Source-only, which is the direct evaluation of a source-trained detector on the target dataset; (2) SN as a baseline to observe how much of the domain gap is caused by size differences; (3) ST3D, the state-of-the-art self-training approach for 3D object detection; (4) Lidar Distillation, an approach that builds on ST3D for the Waymo to nuScenes setting; (5) GT Fine-tune, the best performance we can achieve when we fine-tune the source-trained detector on the target ground-truth labels. We compare methods (1)-(4) with GT fine-tune as it is a more realistic scenario of what is achievable in the presence of perfect pseudo-labels, as opposed to careful selection of the voxel sizes and anchor box dimensions for an “Oracle” supervised benchmark [6]. We fine-tune all models with no frame accumulation. We only compare Lidar Distillation for the target-nuscenes setting as it is designed specifically for the high beam to low beam UDA setting. Though we use SECOND-IoU and CenterPoint for generating pseudo-labels, we only focus on the validation results of SECOND-IoU from different source domains to highlight domain discrepancies.

Evaluation Metric. We follow [5], [6], [26] and adopt the KITTI evaluation metric of Average Precision (AP) over 40 recall positions, in Bird’s Eye View (BEV) and 3D, denoted as AP_{BEV}/AP_{3D} . We assess all models on the “Vehicle” category. For Lyft and nuScenes, we map “truck” and “bus” to the “car” category. We report the AP at Intersection over Union (IoU) thresholds of 0.7 and 0.5 i.e. a vehicle is considered a true positive detection if the IoU of the predicted and ground truth box is over 0.7 or 0.5.

Implementation Details. We train SECOND-IoU [10] and CenterPoint [35] on all datasets and select the best pre-trained model based on evaluating with the source dataset labels. We re-use the same source pre-trained detectors for adapting to all settings. We argue that this is more realistic to real-world applications as we may not have sufficient labels to evaluate and tune the best model for adaptation to a new target dataset. All our models were trained with the OpenPCDet [39] codebase with tweaked settings for voxel size of (0.1m, 0.1m, 0.15m), detection range of $[-75, 75]$ m for x,y axes and $[-2, 4]$ for z-axis, and we shift the point cloud frame

Target: nuScenes				
Method	Source	Detector	IoU=0.7	IoU=0.5
Source-Only	Waymo	SECOND	32.91 / 17.24	43.32 / 37.58
		CenterPoint	32.10 / 17.77	40.83 / 35.77
	Lyft	SECOND	24.15 / 13.47	30.52 / 26.79
		CenterPoint	23.71 / 11.31	30.45 / 26.17
SN [5]	Waymo	SECOND	33.23 / 18.57	43.19 / 37.74
	Lyft	SECOND	27.51 / 17.00	33.32 / 29.92
ST3D [6]	Waymo	SECOND	35.92 / 20.19	43.03 / 38.99
	Lyft	SECOND	29.88 / 18.37	33.18 / 30.67
Lidar Dist. [26]	Waymo	SECOND	42.04 / 24.50	- / -
MS3D (Ours)	Waymo	SECOND	42.23 / 24.76	52.33 / 46.65
	Lyft	SECOND	41.64 / 23.46	51.47 / 45.74
GT Fine-Tune	Waymo	SECOND	44.39 / 29.46	55.61 / 50.83

TABLE II: **UDA from Waymo/Lyft to nuScenes.** We report AP_{BEV}/AP_{3D} . Best results for each source-target pair are highlighted in **bold**. GT Fine-tune uses GT labels to fine-tune the pre-trained detectors with no frame accumulation.

to the ground plane. Lyft and nuScenes pre-trained models were trained with 5 and 10 frame accumulation respectively, following popular practice [3], [4].

For MS3D, we adopt the settings of ST3D [6] and fine-tune all pre-trained detectors with no frame accumulation, for 30 epochs at a learning rate of 1.5×10^{-3} with the Adam one-cycle scheduler. We use pseudo-labels with score threshold of $s > 0.6$ as the ground-truth labels for fine-tuning. For fusing proposals with KBF, we consider a vehicle as present if there are more than 4 box proposals with their centroids within 2m of each other. We use $H = 16$ historical frames for static object refinement and propagate them with a decay of $\beta = 0.95$ with a minimum score $\alpha = 0.7$ if they have more than 7 tracked detections. To focus on static vehicles, we sort Waymo and nuScenes scenes by number of cars and select the top 150 and 190 scenes from nuScenes and Waymo respectively for training; scenes with many cars tend to be carparks. For an unlabelled target domain, this can similarly be done by counting the number of fused 1-frame detections per scene, or by intentionally collecting data from scenes with many parked vehicles. Additionally, this suggests that our model can be further improved with a second round of self-training with the remaining scenes which we leave for future work.

B. Results

As shown in Tables II to IV, our approach outperforms all the other methods regardless of which source domain is used. With nusenes as target domain, MS3D not only improves detections with accurate box localizations (IoU=0.7) and outperforms existing approaches but also greatly increases the number of correct object proposals (IoU=0.5) by a large margin. It can be seen that whilst SN and ST3D improved box localization with IoU=0.7, they did not greatly increase the number of true positive detections as IoU=0.5 remains relatively unchanged. In contrast, MS3D obtains both a high AP_{3D} in IoU=0.7 and IoU=0.5 criterions. In particular, we highlight that for IoU=0.5, MS3D is only $\sim 4AP$ less than the GT Fine-Tune approach, indicating that we can nearly detect all vehicles in the scene. This is also apparent with Waymo as target, Table III, where MS3D obtains a high 42.88 AP_{3D} for IoU=0.7 and 72.34/69.30 AP_{BEV}/AP_{3D} for IoU=0.5 which is $\sim 3AP$ less than GT Fine-Tune.

Target: Waymo				
Method	Source	Detector	IoU=0.7	IoU=0.5
Source-Only	Lyft	SECOND	52.14 / 34.40	61.66 / 58.71
		CenterPoint	50.56 / 31.02	62.32 / 58.97
	nuScenes	SECOND	50.30 / 24.70	61.40 / 53.73
		CenterPoint	49.39 / 24.33	59.52 / 52.64
SN [5]	Lyft	SECOND	53.39 / 39.22	62.42 / 59.55
	nuScenes	SECOND	50.69 / 28.86	61.38 / 53.90
ST3D [6]	Lyft	SECOND	56.06 / 39.17	65.16 / 62.39
	nuScenes	SECOND	55.67 / 28.83	67.19 / 61.63
MS3D (Ours)	Lyft	SECOND	61.25 / 42.88	72.34 / 69.30
	nuScenes	SECOND	61.39 / 42.76	72.47 / 69.45
GT Fine-Tune	nuScenes	SECOND	66.76 / 52.50	75.16 / 72.40

TABLE III: **UDA from nuScenes/Lyft to Waymo.** We report AP_{BEV}/AP_{3D} .

Target: Lyft				
Method	Source	Detector	IoU=0.7	IoU=0.5
Source-Only	Waymo	SECOND	49.68 / 38.94	56.22 / 54.63
		CenterPoint	43.83 / 32.98	49.94 / 48.42
	nuScenes	SECOND	42.22 / 23.62	48.45 / 45.51
		CenterPoint	45.98 / 26.36	52.41 / 49.43
SN [5]	Waymo	SECOND	71.61 / 56.13	80.65 / 78.52
	nuScenes	SECOND	63.11 / 39.60	72.27 / 68.25
ST3D [6]	Waymo	SECOND	73.86 / 56.33	82.90 / 80.81
	nuScenes	SECOND	67.33 / 41.82	77.17 / 72.99
MS3D (Ours)	Waymo	SECOND	76.48 / 61.23	83.36 / 81.49
	nuScenes	SECOND	75.02 / 59.01	83.46 / 81.52
GT Fine-Tune	Waymo	SECOND	81.10 / 66.76	91.12 / 88.69

TABLE IV: **UDA from nuScenes/Waymo to Lyft.** We report AP_{BEV}/AP_{3D} . GT Fine-tune uses Lyft labels to fine-tune the pre-trained detector with no frame accumulation.

With Lyft as the target domain, Table IV, MS3D also outperforms other methods in the IoU=0.7 criterion. We observe however, that the IoU=0.5 performance increase for MS3D is not as large. This is largely due to the lack of annotations in Lyft for objects on both sides of the road and parked vehicles at a distance, as noted by [6]. As a result, correct proposals by MS3D will be penalized as false positives, which makes it challenging to accurately assess. From the above results, we have demonstrated that MS3D is able to adapt detectors from low (e.g. nuScenes) to high (e.g. Waymo) beam lidar datasets and vice-versa, unlike ST3D [6] and Lidar Distillation [26].

For each target domain, we show the detection performance from two different source domains. We demonstrate that MS3D, regardless of the source-trained detector used as the pre-trained model, can be fine-tuned to a similar state-of-the-art performance. For instance, with ST3D, selecting nuScenes pre-trained detector for self-training to Waymo (Table III) leads to 10.34 AP_{3D} less in IoU=0.7 compared to selecting Lyft. With MS3D, the choice of pre-trained source detector is an insignificant difference of 0.12 AP_{3D} between selecting either Lyft or nuScenes. This outcome of MS3D is particularly beneficial in real-world scenarios where obtaining enough labelled data for robust evaluation of the self-trained model can be expensive.

C. Ablation

Pseudo-label Quality. In Fig. 6, we show that our pseudo-labels consistently improve the detections of every source-trained detector on the target domain. When we combine all

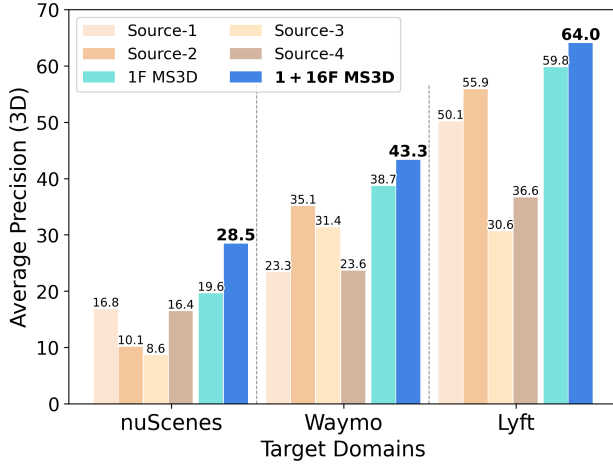


Fig. 6: Evaluation of MS3D’s pseudo-labels on different target domains. 1F MS3D refers to using only KBF on 1-frame detections from the 4 source domains. 1+16F MS3D refers to our final pseudo-labels after refining static vehicles.

4 sources with KBF, we can already surpass the best source-trained detector’s AP_{3D} . By adding 16-frame detections for refining of static vehicles, we can further boost the detection by an impressive amount for all target domains. For example with nuScenes as the target domain, MS3D overcomes the detection range limitations of a sparse-beam lidar with our multi-frame static refinement, leading to a 8.84 AP_{3D} increase from 1F MS3D to 1F+16F MS3D.

KDE Box Fusion. We compare KBF with NMS [32] and two variants of Weighted Box Fusion [34] in Table V. WBF-C is the official 3D implementation using opposite 3D box corners, and WBF-P is weighted average of box params ($c_{xyz}, d_x, d_y, d_z, \theta_y, s$). We show that KBF outperforms other methods at all ranges, with the 50-80m range having the most improvement over existing methods. With KDE, setting a high bandwidth is similar to taking the average of the data points. Being able to tune the bandwidth for different parameters allows us to better capture the nuances of the box fusion process. For example, a common error in box prediction is the heading orientation being incorrect by an error of π . Setting a high bandwidth for rotation estimation would therefore be detrimental as we may select an in-between orientation instead of one that corrects the orientation by π .

Static Object Refinement. In Table VI, we show that using 16-frame detections for static objects gives a mild improvement over 1F MS3D (i.e., using KBF for 1-frame detections). Applying KBF on H historical boxes of a static object can further improve the localization of the box. As explained in Section III-E, using a single box is suboptimal due to ego-pose drift, which is reflected in the lower performance compared to using $H = 16$ boxes. Quantifying the extent of this difference is challenging because comparing $H=16$ and “Single box” to a GT label may only differ by a few cm, which can still meet the $IoU=0.7$ threshold. The ego-pose drift becomes problematic when there are only a sparse number of points on the car, as a few cm difference could result in the exclusion of the car’s points entirely. Therefore, based on qualitative and quantitative assessment, we chose to

Method	IoU=0.7	RANGE (L2/APH)		
	AP_{BEV}/AP_{3D}	[0,30]	[30,50]	[50,+inf]
nuScenes / CenterPoint	49.49 / 23.33	58.80	17.56	1.89
nuScenes / SECOND	50.74 / 23.64	60.07	15.56	1.61
Lyft / CenterPoint	49.26 / 31.35	61.53	30.97	9.88
Lyft / SECOND	50.83 / 35.09	46.98	19.11	6.93
NMS [32]	57.93 / 34.88	57.13	24.01	7.59
WBF-C [34]	53.27 / 36.55	67.17	32.74	8.33
WBF-P [34]	54.44 / 36.75	67.43	33.32	8.92
KBF (Ours)	57.22 / 38.67	68.89	33.93	10.40

TABLE V: Ablation study of box fusion methods for multiple detector predictions on Waymo as target domain.

Method	IoU=0.7	RANGE (L2/APH)		
	AP_{BEV}/AP_{3D}	[0,30]	[30,50]	[50,+inf]
nuScenes / CenterPoint	49.49 / 23.33	58.80	17.56	1.89
nuScenes / SECOND	50.74 / 23.64	60.07	15.56	1.61
Lyft / CenterPoint	49.26 / 31.35	61.53	30.97	9.88
Lyft / SECOND	50.83 / 35.09	46.98	19.11	6.93
1F MS3D	57.22 / 38.67	68.89	33.93	10.4
$H = 0$	59.19 / 38.73	69.49	34.47	10.63
$H = 4$	62.06 / 40.89	71.74	38.83	14.11
$H = 16$	62.32 / 43.33	72.23	41.72	17.63
Single box	62.32 / 43.12	72.02	41.30	17.88

TABLE VI: Ablation study of our static box labelling using a rolling window of H frames for KBF on Waymo as target domain. For $H = 0$ we replace static boxes with their 16-frame detections. For “Single box”, we use KBF of all observed frames.

use $H = 16$ boxes for estimating the static box for a vehicle to minimise the impact of ego-pose drift.

D. Discussion

In our experimentation with various source to target domain pairs, we observed that while 16-frame accumulation increased point density, it did not necessarily help detectors localize well even when the entire car shape is visible. For example, when testing nuScenes/Waymo detectors on KITTI, we found that for a fully visible, 16-frame accumulated car at 5m away from the ego vehicle, detectors consistently predicted a box that was 0.5-1m longer. This was also observed when using a KITTI detector on nuScenes/Waymo where it would predict a smaller box that did not encapsulate the entire object. We attribute this largely to the scan pattern domain gap as 16-frame accumulated point clouds appear quite distinct depending on the lidar used. In such cases where target dataset statistics is known to deviate significantly from the source dataset, we recommend incorporating Random Object Scaling [6] or SN in the self-training process.

V. CONCLUSION

In this paper, we introduce MS3D, a self-training pipeline that utilizes multiple source domains and temporal information to adapt to new target domains. As multiple labelled datasets are often available in real-world applications, we show that combining detectors trained on these sources can effectively auto-label an unlabelled target dataset and fine-tune the source detector for improved performance. MS3D achieves state-of-the-art results on all tested UDA settings. Our proposed KBF method consistently improves pseudo-label quality, surpassing the performance of the best individual source detector. However, the optimal combination of

detectors for an unlabelled target domain remains an open question, which we leave as future work.

REFERENCES

- [1] A. Geiger, P. Lenz, and R. Urtasun, "Are we ready for autonomous driving? the kitti vision benchmark suite," in *2012 IEEE Conference on Computer Vision and Pattern Recognition*. IEEE, 2012, pp. 3354–3361.
- [2] P. Sun, H. Kretschmar, X. Dotiwalla, A. Chouard, V. Patnaik, P. Tsui, J. Guo, Y. Zhou, Y. Chai, B. Caine, et al., "Scalability in perception for autonomous driving: Waymo open dataset," in *Proceedings of the IEEE/CVF Conference on Computer Vision and Pattern Recognition*, 2020, pp. 2446–2454.
- [3] H. Caesar, V. Bankiti, A. H. Lang, S. Vora, V. E. Liong, Q. Xu, A. Krishnan, Y. Pan, G. Baldan, and O. Beijbom, "nusenes: A multimodal dataset for autonomous driving," in *Proceedings of the IEEE/CVF Conference on Computer Vision and Pattern Recognition*, 2020, pp. 11 621–11 631.
- [4] R. Kesten, M. Usman, J. Houston, T. Pandya, K. Nadhamuni, A. Ferreira, M. Yuan, B. Low, A. Jain, P. Ondruska, S. Omari, S. Shah, A. Kulkarni, A. Kazakova, C. Tao, L. Platinsky, W. Jiang, and V. Shet, "Woven planet perception dataset 2020," <https://www.woven-planet.global/en/data/perception-dataset>, 2019.
- [5] Y. Wang, X. Chen, Y. You, L. E. Li, B. Hariharan, M. Campbell, K. Q. Weinberger, and W.-L. Chao, "Train in germany, test in the usa: Making 3d object detectors generalize," in *Proceedings of the IEEE/CVF Conference on Computer Vision and Pattern Recognition*, 2020, pp. 11 713–11 723.
- [6] J. Yang, S. Shi, Z. Wang, H. Li, and X. Qi, "St3d: Self-training for unsupervised domain adaptation on 3d object detection," in *Proceedings of the IEEE/CVF Conference on Computer Vision and Pattern Recognition*, 2021, pp. 10 368–10 378.
- [7] Z. Yang, Y. Zhou, Z. Chen, and J. Ngiam, "3d-man: 3d multi-frame attention network for object detection," in *Proceedings of the IEEE/CVF Conference on Computer Vision and Pattern Recognition*, 2021, pp. 1863–1872.
- [8] C. R. Qi, Y. Zhou, M. Najibi, P. Sun, K. Vo, B. Deng, and D. Anguelov, "Offboard 3d object detection from point cloud sequences," in *Proceedings of the IEEE/CVF Conference on Computer Vision and Pattern Recognition*, 2021, pp. 6134–6144.
- [9] X. Chen, S. Shi, B. Zhu, K. C. Cheung, H. Xu, and H. Li, "Mppnet: Multi-frame feature intertwining with proxy points for 3d temporal object detection," in *Computer Vision—ECCV 2022: 17th European Conference, Tel Aviv, Israel, October 23–27, 2022, Proceedings, Part VIII*. Springer, 2022, pp. 680–697.
- [10] Y. Yan, Y. Mao, and B. Li, "Second: Sparsely embedded convolutional detection," *Sensors*, vol. 18, no. 10, p. 3337, 2018.
- [11] A. H. Lang, S. Vora, H. Caesar, L. Zhou, J. Yang, and O. Beijbom, "Pointpillars: Fast encoders for object detection from point clouds," in *Proceedings of the IEEE/CVF Conference on Computer Vision and Pattern Recognition*, 2019, pp. 12 697–12 705.
- [12] S. Shi, X. Wang, and H. Li, "Pointcnn: 3d object proposal generation and detection from point cloud," in *Proceedings of the IEEE/CVF Conference on Computer Vision and Pattern Recognition*, 2019, pp. 770–779.
- [13] C. R. Qi, H. Su, K. Mo, and L. J. Guibas, "Pointnet: Deep learning on point sets for 3d classification and segmentation," in *Proceedings of the IEEE Conference on Computer Vision and Pattern Recognition*, 2017, pp. 652–660.
- [14] S. Shi, C. Guo, L. Jiang, Z. Wang, J. Shi, X. Wang, and H. Li, "Pvrcnn: Point-voxel feature set abstraction for 3d object detection," in *Proceedings of the IEEE/CVF Conference on Computer Vision and Pattern Recognition*, 2020, pp. 10 529–10 538.
- [15] T. Yin, X. Zhou, and P. Krahenbuhl, "Center-based 3d object detection and tracking," in *Proceedings of the IEEE/CVF conference on computer vision and pattern recognition*, 2021, pp. 11 784–11 793.
- [16] C. Qin, L. Wang, Y. Zhang, and Y. Fu, "Generatively inferential co-training for unsupervised domain adaptation," in *Proceedings of the IEEE/CVF International Conference on Computer Vision Workshops*, 2019, pp. 0–0.
- [17] K. Saito, Y. Ushiku, T. Harada, and K. Saenko, "Strong-weak distribution alignment for adaptive object detection," in *Proceedings of the IEEE/CVF Conference on Computer Vision and Pattern Recognition*, 2019, pp. 6956–6965.
- [18] L. Yi, B. Gong, and T. Funkhouser, "Complete & label: A domain adaptation approach to semantic segmentation of lidar point clouds," in *Proceedings of the IEEE/CVF Conference on Computer Vision and Pattern Recognition*, 2021, pp. 15 363–15 373.
- [19] Y. Zou, Z. Yu, B. Kumar, and J. Wang, "Unsupervised domain adaptation for semantic segmentation via class-balanced self-training," in *Proceedings of the European Conference on Computer Vision (ECCV)*, 2018, pp. 289–305.
- [20] A. Tarvainen and H. Valpola, "Mean teachers are better role models: Weight-averaged consistency targets improve semi-supervised deep learning results," *Advances in neural information processing systems*, vol. 30, 2017.
- [21] Z. Luo, Z. Cai, C. Zhou, G. Zhang, H. Zhao, S. Yi, S. Lu, H. Li, S. Zhang, and Z. Liu, "Unsupervised domain adaptive 3d detection with multi-level consistency," in *Proceedings of the IEEE/CVF International Conference on Computer Vision*, 2021, pp. 8866–8875.
- [22] D. Tsai, J. S. Berrio, M. Shan, S. Worrall, and E. Nebot, "See eye to eye: A lidar-agnostic 3d detection framework for unsupervised multi-target domain adaptation," *IEEE Robotics and Automation Letters*, vol. 7, no. 3, pp. 7904–7911, 2022.
- [23] D. Tsai, J. S. Berrio, M. Shan, E. Nebot, and S. Worrall, "Viewer-centred surface completion for unsupervised domain adaptation in 3d object detection," *arXiv preprint arXiv:2209.06407*, 2022.
- [24] Y. You, C. A. Diaz-Ruiz, Y. Wang, W.-L. Chao, B. Hariharan, M. Campbell, and K. Q. Weinberger, "Exploiting playbacks in unsupervised domain adaptation for 3d object detection in self-driving cars," in *2022 International Conference on Robotics and Automation (ICRA)*. IEEE, 2022, pp. 5070–5077.
- [25] Z. Li, Z. Chen, A. Li, L. Fang, Q. Jiang, X. Liu, and J. Jiang, "Unsupervised domain adaptation for monocular 3d object detection via self-training," in *Computer Vision—ECCV 2022: 17th European Conference, Tel Aviv, Israel, October 23–27, 2022, Proceedings, Part IX*. Springer, 2022, pp. 245–262.
- [26] Y. Wei, Z. Wei, Y. Rao, J. Li, J. Zhou, and J. Lu, "Lidar distillation: Bridging the beam-induced domain gap for 3d object detection," *arXiv preprint arXiv:2203.14956*, 2022.
- [27] S. M. Ahmed, D. S. Raychaudhuri, S. Paul, S. Oymak, and A. K. Roy-Chowdhury, "Unsupervised multi-source domain adaptation without access to source data," in *Proceedings of the IEEE/CVF conference on computer vision and pattern recognition*, 2021, pp. 10 103–10 112.
- [28] J. Dong, Z. Fang, A. Liu, G. Sun, and T. Liu, "Confident anchor-induced multi-source free domain adaptation," *Advances in Neural Information Processing Systems*, vol. 34, pp. 2848–2860, 2021.
- [29] J. He, X. Jia, S. Chen, and J. Liu, "Multi-source domain adaptation with collaborative learning for semantic segmentation," in *Proceedings of the IEEE/CVF Conference on Computer Vision and Pattern Recognition*, 2021, pp. 11 008–11 017.
- [30] X. Yao, S. Zhao, P. Xu, and J. Yang, "Multi-source domain adaptation for object detection," in *Proceedings of the IEEE/CVF International Conference on Computer Vision*, 2021, pp. 3273–3282.
- [31] B. Zhang, J. Yuan, B. Shi, T. Chen, Y. Li, and Y. Qiao, "Uni3d: A unified baseline for multi-dataset 3d object detection," *arXiv preprint arXiv:2303.06880*, 2023.
- [32] A. Neubeck and L. Van Gool, "Efficient non-maximum suppression," in *18th international conference on pattern recognition (ICPR'06)*, vol. 3. IEEE, 2006, pp. 850–855.
- [33] N. Bodla, B. Singh, R. Chellappa, and L. S. Davis, "Soft-nms—improving object detection with one line of code," in *Proceedings of the IEEE international conference on computer vision*, 2017, pp. 5561–5569.
- [34] R. Solovyev, W. Wang, and T. Gabruseva, "Weighted boxes fusion: Ensembling boxes from different object detection models," *Image and Vision Computing*, vol. 107, p. 104117, 2021.
- [35] T. Yin, X. Zhou, and P. Krahenbuhl, "Center-based 3d object detection and tracking," in *Proceedings of the IEEE/CVF conference on computer vision and pattern recognition*, 2021, pp. 11 784–11 793.
- [36] E. Parzen, "On estimation of a probability density function and mode," *The annals of mathematical statistics*, vol. 33, no. 3, pp. 1065–1076, 1962.
- [37] Z. Pang, Z. Li, and N. Wang, "Simpletrack: Understanding and rethinking 3d multi-object tracking," *arXiv preprint arXiv:2111.09621*, 2021.
- [38] X. Weng, J. Wang, D. Held, and K. Kitani, "3D Multi-Object Tracking: A Baseline and New Evaluation Metrics," *IROS*, 2020.
- [39] O. D. Team, "Openpcdet: An open-source toolbox for 3d object detection from point clouds," <https://github.com/open-mmlab/OpenPCDet>, 2020.